

1   **Mitochondrial behaviour throughout the lytic cycle of *Toxoplasma gondii***

2

3

4   Jana Ovciarikova<sup>1</sup>, Leandro Lemgruber<sup>1</sup>, Krista L. Stilger<sup>2</sup>, William J. Sullivan

5   Jr.<sup>2,3</sup> and Lilach Sheiner<sup>1\*</sup>

6

7   <sup>1</sup>Wellcome Trust Centre for Molecular Parasitology, University of Glasgow, UK

8   <sup>2</sup>Department of Pharmacology and Toxicology, Indiana University School of  
9   Medicine, Indianapolis, Indiana 46202, USA

10   <sup>3</sup>Department of Microbiology and Immunology, Indiana University School of  
11   Medicine, Indianapolis, Indiana 46202, USA

12   \*Corresponding author: [lilach.sheiner@glasgow.ac.uk](mailto:lilach.sheiner@glasgow.ac.uk)

13

14   Keywords:

15   Mitochondria, Organelle, Morphology, Parasite, Toxoplasma, Lytic-cycle, Alveoli,  
16   Inner-membrane-complex, membrane contact sites.

17

18

19

20 **Abstract**

21

22 Mitochondria distribution in cells controls cellular physiology in health and  
23 disease. Here we describe the mitochondrial morphology and positioning found  
24 in the different stages of the lytic cycle of the eukaryotic single-cell parasite  
25 *Toxoplasma gondii*. The lytic cycle, driven by the tachyzoite life stage, is  
26 responsible for acute toxoplasmosis. It is known that whilst inside a host cell the  
27 tachyzoite maintains its single mitochondrion at its periphery. We found that upon  
28 parasite transition from the host cell to the extracellular matrix, mitochondrion  
29 morphology radically changes, resulting in a reduction in peripheral proximity.  
30 This change is reversible upon return to the host, indicating that an active  
31 mechanism maintains the peripheral positioning found in the intracellular stages.  
32 Comparison between the two states by electron microscopy identified regions of  
33 coupling between the mitochondrion outer membrane and the parasite pellicle,  
34 whose features suggest the presence of membrane contact sites, and whose  
35 abundance changes during the transition between intra- and extra-cellular states.  
36 These novel observations pave the way for future research to identify molecular  
37 mechanisms involved in mitochondrial distribution in *Toxoplasma* and the  
38 consequences of these mitochondrion changes on parasite physiology.

39

40 **Introduction**

41

42 The various functions of mitochondria are governed in part by positioning of the  
43 organelle at relevant cellular locations. The dynamic nature of mitochondrial  
44 behavior is indicated by the multiple morphologies seen in various cell types and  
45 under various growth conditions. For example, several mammalian cell-types  
46 show morphologically heterogeneous and unconnected mitochondria in a steady  
47 state<sup>1</sup>. On the other hand, mitochondria can assume a highly connected tubular  
48 structure, e.g. during the development of cardiomyocytes<sup>2</sup>; or a highly  
49 fragmented morphology as in the case of yeast sporulation<sup>3</sup>. In another example,  
50 the eukaryotic parasite *Trypanosoma brucei* presents a small, unbranched tube-  
51 like mitochondrion during the life-cycle stage when it is not involved in ATP  
52 production and a branched mitochondrion when the TCA cycle is active<sup>4 5 6</sup>. Little  
53 is known about morphological changes that may occur in the mitochondrion of  
54 the eukaryotic unicellular parasite *Toxoplasma gondii* (*T. gondii*). Examination of  
55 mitochondrial morphology in the rapidly replicating life stage (tachyzoite), when  
56 intracellular, shows a single mitochondrion which is predominantly found in a  
57 lasso shape that spans the parasite periphery<sup>7,8</sup>. This lasso shape is the main  
58 morphology described for the *Toxoplasma* mitochondrion in the current literature.  
59 Interestingly, during tachyzoite cell division the mother mitochondrion maintains  
60 close proximity to the mother-cell periphery and is excluded from the growing  
61 daughters until the late stages of cytokinesis<sup>9</sup>.

62 *T. gondii* must reside within a nucleated host cell to grow and divide. The

63 tachyzoite stage will spend time in the extracellular environment after egress  
64 from a host cell, when it seeks a new host cell to invade, and thus continues its  
65 “lytic cycle”. Recent observations suggest that extracellular tachyzoites are also  
66 found free in the blood stream of infected mice<sup>10</sup>. The transition from intracellular  
67 to extracellular conditions is accompanied by drastic changes in ion  
68 concentration and nutrient availability. The ability to survive outside the host cell,  
69 move around and then invade a new host cell is critical to the *T. gondii* lifestyle  
70 and virulence.

71

72 As a first step to tease out a potential function-morphology correlation in the *T.*  
73 *gondii* mitochondrion, we looked for any morphological changes that can be  
74 observed during the lytic cycle. We found that extracellular parasites exhibit  
75 drastic changes in mitochondrial morphology immediately after being released  
76 from the host cells. These changes are characterized by detachment of the  
77 mitochondrial tubule from the parasite periphery and its accumulation in  
78 concentrated regions in the cell. These changes seem directional and reversible  
79 upon host cell re-entry. Electron microscopy links these striking morphological  
80 dynamics to a change in the abundance of long patches of high proximity  
81 between the parasite’s mitochondrion and the parasite’s alveoli-sacs at its  
82 pellicle. These observations pave the way for future studies of the molecular  
83 mechanisms controlling apicomplexan mitochondrial behavior and how it  
84 contributes to survival of parasites between intra- and extracellular states.

85

86 **Results**

87

88 **Morphological changes in the mitochondrion of extracellular tachyzoites**

89

90 Most previously available imaging of mitochondrial morphology and dynamics in  
91 live *T. gondii* utilized a matrix marker whereby the leader sequence of  
92 mitochondrial HSP60 is fused to the red fluorescent protein and the resulting  
93 fusion is expressed from a heterologous promoter<sup>9</sup>. We generated a fluorescent  
94 marker for the mitochondrial periphery via fusion of the TGME49\_215430  
95 encoded protein<sup>11</sup> to the yellow fluorescent protein (YFP) by endogenous  
96 tagging. This protein was found in a search for *T. gondii* proteins that contain  
97 each a single hydrophobic domain, and within this screen it was localized to the  
98 mitochondrion (Sheiner and Soldati unpublished work). Homologs of this protein  
99 are only found in organisms from the Alveolata group (that includes within it the  
100 phylum Apicomplexa to which *T. gondii* belongs). No functional domains are  
101 predicted; however a lipid attachment site is predicted at the N-terminus  
102 (<http://prosite.expasy.org/PS51257>) that suggest potential attachment to the  
103 mitochondrial membrane. TGME49\_215430 endogenously tagged with YFP  
104 (215430-YFP) co-localizes with the outer-mitochondrial membrane marker  
105 Tom40<sup>12</sup> as well as the signal obtained from Mitotracker® (Figure 1a,b). We  
106 observed that imaging with this marker identifies mitochondrial structures that are  
107 not labeled using the matrix marker (Figure 1c, arrowhead). It further labels a

108 continuous mitochondrial tubule, whereas the matrix signal is fragmented (Figure  
109 1d, arrowheads). 215430-YFP is used throughout this report.  
110 We revisited the previous observation on mitochondrial morphology in  
111 intracellular parasites. First we validated the new marker by reproducing the  
112 observations of the unique mitochondrial behavior in dividing tachyzoites<sup>9</sup> (Figure  
113 S1a,b,c, Movie S1). Next, we scored morphologies in intracellular parasites. *T.*  
114 *gondii* intracellular replication is asynchronous and different parasites are at  
115 different stages of the cell cycle at a given time. Nevertheless, we observed that  
116 an average of 94% of intracellular parasites possess the typical lasso shaped  
117 mitochondria with peripheral localization (Figure 2), supporting earlier  
118 observations that this is the predominant morphology maintained throughout the  
119 intracellular cell cycle<sup>7</sup>. Live imaging show that the majority of parasites contain a  
120 lasso shaped mitochondrion also just before egress (Movie S2). However, due to  
121 the constant movement of the parasites within cells in the Z axis during imaging  
122 we were unable to determine the mitochondrial morphology with accuracy in all  
123 the parasites, making quantification difficult. In contrast, we found that  
124 immediately after host cell egress, *T. gondii* mitochondria present an array of  
125 morphologies (Figure 2a,b), only 35% of which retain the lasso shape (Figure  
126 2c). We assigned these extracellular mitochondrial morphologies to three main  
127 categories based on their shapes and termed them “lasso”, “sperm-like” and  
128 “collapsed” (Figure 2d). An average of 42% of freshly released parasites have  
129 “sperm-like” mitochondria (Figure 2c), which consist of a round bundle of folded  
130 mitochondrial tubule, with a part of the tubule remaining extended. 21% of

131 extracellular parasites show completely collapsed mitochondrial tubules (Figure  
132 2c). Similar distribution of these three morphologies are also observed when  
133 parasites egress into diluted medium that better mimics the low nutrient  
134 environment encountered by the parasite in the extracellular matrix *in*  
135 *vivo*<sup>13</sup>(Figure 2c). Equally, similar distribution of these morphologies is observed  
136 when parasites egress is induced via the calcium ionophore, ionomycin (Figure  
137 2c), with a moderate elevation in the proportion of collapsed mitochondria.

138

139 Changes in mitochondrial morphology were observed in *T. gondii* previously, in  
140 response to starvation and drug treatment. These studies describe mitochondrial  
141 swelling and fragmentation observed after 6 or 8 hours of treatment<sup>14 15</sup>. We  
142 noticed occasional freshly egressed parasites showing fragmentation or swelling  
143 similar to what was observed following starvation or drug treatment. In all cases,  
144 unlike the lasso, sperm-like and collapsed forms, this was coupled to an overall  
145 abnormal cell morphology documented by brightfield imaging (Figure S2a).  
146 Comparison of these morphologies via super-resolution microscopy (3D-SIM)  
147 using the peripheral marker 215430-YFP showed that swollen and fragmented  
148 mitochondria have different structures to the packed folded tubule observed  
149 immediately upon host-cell release (Figure S2b). Furthermore, extracellular  
150 parasites with swollen and fragmented mitochondria stain with propidium-iodide  
151 (PI), indicating cell death has commenced. Additionally, their mitochondria are  
152 not labelled with Mitotracker®, suggesting they are no longer active (Figure

153 S2c,d). Parasites with fragmented or swollen mitochondria were thus excluded  
154 from our analysis.

155

156 **Mitochondrion morphology during extracellular gliding motility, host cell**  
157 **invasion, and entry into a new host cell.**

158

159 During the lytic cycle (Figure 3a), extracellular tachyzoites use gliding motility to  
160 find and enter their next host cell. We examined mitochondrial morphology in  
161 moving parasites upon temperature-shift induction of gliding motility in fresh  
162 mechanically-released parasites. The repertoire of morphologies in gliding  
163 parasites is similar to that of the overall population of freshly released parasites  
164 (33% lasso, 50% sperm-like and 17% collapsed) with no significant difference in  
165 the frequencies of each shape (Figures 3b,c, Movie S3).

166 Host cell invasion is the next essential step of the *T. gondii* lytic cycle (Figure 3a).  
167 Using the green/red assay (<sup>16</sup>, Movie S4.1/2/3) to label invading parasites (Figure  
168 3d), we scored parasites that were in the act of invasion. We found a similar  
169 distribution of morphologies to those found in freshly egressed and in gliding  
170 parasites (33% lasso, 55% sperm-like and 12% collapsed), albeit a moderate  
171 increase in the frequency of sperm-like shaped mitochondria in the invading  
172 population (Figure 3e).

173 Finally, parasites presenting the collapsed mitochondrial tubule morphology were  
174 analyzed after entry into a new host cell. Following invasion, collapsed  
175 mitochondria re-expand and re-establish the typical intracellular lasso shape

176 (Figure 4a, Movie S5). Among three independent live-imaging experiments the  
177 timing of re-expansion after invasion varied. However, cell division (as visualized  
178 by the appearance of daughter cells) occurred only after mitochondrial  
179 remodeling into a lasso shape (Figure 4a, Movie S5). In this context it is worth  
180 mentioning that when examining cultures of intracellular parasites, the 0.7% that  
181 contain a collapsed mitochondrion (Figure 2c) are always single parasites. We  
182 propose that these are parasites that recently invaded the host cell, and have not  
183 yet remodeled their mitochondrion to the lasso shape.

184 Interestingly, the transition from collapsed to lasso involves an intermediate  
185 sperm-like shape (Figure 4a arrowhead). Due to the rapid motility of extracellular  
186 parasites we were unable to capture the remodeling in the opposite direction  
187 (from lasso to collapsed) via time-lapse microscopy of freshly egressed  
188 parasites. However, we found that parasites that remain extracellular for 0, 6, 12  
189 and 24 hours, and that do not possess swollen and fragmented mitochondria,  
190 show 37%, 9.3%, 3.7% and 1.5% lasso-shaped mitochondria respectively  
191 (Figure 4b). Within these time points the number of parasites with sperm-like  
192 mitochondria initially increased (from 45.5% to 66.2% at 6 hours) and then  
193 droped (to 27.8% at 24 hours), while parasites with collapsed mitochondria  
194 gradually accumulated to become 70.7% at 24 hours (Figure 4b). This dynamic  
195 suggests a model whereby the sperm-like morphology is an intermediate form  
196 between lasso and collapsed. Analysis of the orientation of the tubule extension  
197 (“tail”) of the sperm-like mitochondria showed that the tail is predominantly basal  
198 (Figure 4c), suggesting that the retraction from lasso to sperm-like is directional.

199

200 Collectively, these observations show that mitochondrial morphology in *T. gondii*  
201 tachyzoites is dynamic during the lytic cycle. The mitochondrion responds to the  
202 transitions between extracellular and intracellular stages in a controlled manner  
203 that results in the remodeling into a lasso shape observed after host cell  
204 invasion.

205

206 **Patches of tight mitochondrion-pellicle proximity are observed, and their**  
207 **abundance correlates with mitochondrial remodeling**

208

209 We investigated the cellular structures linked to the peripheral positioning of the  
210 mitochondrion in intracellular tachyzoites. The behavior of mitochondria in other  
211 eukaryotic cells is controlled via several molecular mechanisms<sup>17</sup>. In many  
212 systems, components of the cell cytoskeleton play a central role in this process.  
213 We assessed mitochondrial morphology in response to treatment with the  
214 microtubule destabilization agent Oryzalin. Fixed cell microscopy showed that  
215 while this treatment results in irregular mitochondrion morphology, the results  
216 were distinct from the above described morphologies in extracellular parasites  
217 (Figure S3a). Moreover, live-imaging of tachyzoite cell division under Oryzalin  
218 treatment shows that mitochondria enter the new daughter cells while still  
219 forming lasso-like shapes (Figure S3b arrowheads, Movie S6).

220

221 Mitochondrial morphology is also shaped through its interactions with other

222 organelles. We investigated whether other organelles show behavior that may be  
223 linked to the observed mitochondrial morphology changes upon the transition  
224 from intracellular to extracellular stages. We analyzed the morphologies and  
225 distribution of the three other organelles that occupy a large part of the tachyzoite  
226 cell and that show association with the mitochondrion in intracellular parasites<sup>7</sup>:  
227 the rhoptries, parasite-specific organelles that stretch from the apical tip to the  
228 nucleus; the nucleus; and the endoplasmic reticulum (ER) (Figure 5a). No clear  
229 correlation between the positioning or morphology changes of these organelles  
230 and that of the mitochondrion was apparent (data not shown). We further  
231 examined the apicoplast, a relict plastid that shares metabolic pathways with the  
232 mitochondrion (reviewed e.g. in<sup>18</sup>), and for which an association with the  
233 mitochondrion is well-documented<sup>9,19</sup>. Specifically, we examined if the apicoplast  
234 is consistently found at a certain end of the sperm-like mitochondrion or at a  
235 certain end or distance from the collapsed mitochondrion. We further tested  
236 whether the apicoplast shape or location within the cell changes along with the  
237 mitochondrial shape-change. Again, no clear correlation was apparent (data not  
238 shown). However, imaging with the mitochondrial peripheral marker and a  
239 parasite pellicle marker (IMC3) revealed that all three extracellular morphologies  
240 show a trend of mitochondrial retraction from the tachyzoite periphery (Figure  
241 5b).

242

243 The pellicle of *T. gondii* is multilayered (Figure 6a Scheme); underneath the  
244 plasma membrane lays the inner membrane complex (IMC)<sup>20</sup>. The IMC is made

245 up of flattened membrane sacs termed alveoli, covered, on the cytoplasmic face,  
246 by a network of intermediate filament-like proteins named the subpellicular  
247 network<sup>21</sup>. The IMC encircles the parasite periphery with openings only at the  
248 apical end (Figure 6a Scheme) making it a strong candidate to interact with the  
249 mitochondrion and anchor its peripheral position in intracellular parasites. In  
250 support of this hypothesis, super-resolution microscopy showed substantial  
251 overlap in the signal from these two compartments (Figure 5b, Figure S1c  
252 arrowheads), which suggests proximity of less than 200nm in the regions of  
253 overlap. Immuno-electron microscopy using cryofixation and labeling the outer  
254 mitochondrial membrane marker protein TgElp3<sup>22</sup>(Figure 6b), as well as electron  
255 tomography (Figure S4), detected an abundance of regions of juxtaposition of  
256 mitochondrion and IMC, whereby the membranes of both organelles maintain  
257 constant distance (of less than 50nm) over stretches of 100nm-1000nm. Among  
258 254 random EM images of intracellular parasite sections, 39.8% presented the  
259 mitochondria within these patches of tight constant distance from the IMC; 41.3%  
260 presented more distant mitochondria; and 18.9% did not contain any  
261 mitochondria profile in the section (Figure 6c). Within the images showing  
262 stretches of mitochondrion-IMC proximity of less than 50nm, we measured an  
263 average distance of 26.23 nm (+/- 12.02 nm). On the other hand, analysis of 240  
264 EM images from freshly egressed extracellular parasites revealed 28.6% cases  
265 of mitochondrion-IMC alignment, while 51.4% showed no tight association and  
266 20% showing no mitochondria profile in the section (Figure 6c). The average

267 distance between the IMC and mitochondria at the patches of alignment seen in  
268 extracellular parasites was 30.28 nm (+/- 12.33nm).

269 Finally, we tested whether the observed points of contact are stable over time by  
270 performing time-lapse microscopy with frequent imaging time points (every 10  
271 seconds). We could image for periods of 10-30 minutes during which we  
272 observed contacts that lasted through the whole duration of the imaging (Figure  
273 6d, square parentheses, Movie S7) and up to 30 minutes. Occasional transient  
274 (no longer than 30 seconds) extensions towards the basal and apical end of the  
275 parasite as well as inward in the direction of the nucleus are also observed  
276 (Figure 6d, arrowheads).

277

278 Collectively, these data show that the mitochondrion aligns closely with the IMC,  
279 and that this alignment is more extensive in intracellular parasites. We propose  
280 that this intimate association contribute to the mitochondrion shape and  
281 positioning seen in intracellular tachyzoites.

282

283 **Discussion**

284

285 We describe new mitochondrial behavior in the protozoan parasite *T. gondii*  
286 whereby the transition between extracellular and intracellular stages induces  
287 changes in the organelle's morphology. We identified three distinct morphological  
288 states that occur in extracellular tachyzoites and that are spotted immediately  
289 upon host cell egress; each state is observed with similar frequency in both the  
290 commonly used *in vitro* growth medium as well as a nutrient-reduced medium  
291 that more closely mimics the extracellular matrix *in vivo* (Figure 2). Likewise, the  
292 distribution of these morphologies is seen in both moving and in actively invading  
293 parasites (Figure 3). Finally, the change is reversible as collapsed mitochondria  
294 remodel into the typical lasso shape upon re-entry into the host. Taken together,  
295 these data suggest that the observed changes have physiological and functional  
296 significance.

297

298 Our observations point out a distinction between intracellular and extracellular  
299 mitochondrial morphology. The comparison between the two provided us with an  
300 opportunity to begin a dissection of the cellular features that may mediate the  
301 typical lasso shape of the mitochondria of intracellular tachyzoites. We did this by  
302 attempting to find a link between the behavior of certain cellular structures and  
303 the mitochondrial morphology. Mitochondrial morphology and localization in cells  
304 is controlled via interactions with components of the cytoskeleton and through

305 interactions with other organelles<sup>17</sup>. Our analyses thus focused on both these  
306 factors.

307 Previous studies have shown that actin disruption results in morphological  
308 defects in mitochondria in both *T. gondii*<sup>23</sup> and in the related parasite  
309 *Plasmodium falciparum*<sup>24</sup>. Likewise, treatments with microtubule stability  
310 inhibitors affect mitochondrial morphology (<sup>9</sup>, Figure S3). However, the peripheral  
311 distribution of the mitochondrion is still observed under both these treatments,  
312 and the three morphological states seen in extracellular parasite are not  
313 reproduced. Moreover, we recorded the formation of lasso-like shaped  
314 mitochondria when Oryzalin treated parasites divide (Figure S3, Movie S6). We  
315 conclude that while components of the cytoskeleton appear to contribute to the  
316 control of mitochondrial morphology, additional factors are likely to be involved in  
317 mediating the peripheral positioning of the mitochondrion of intracellular  
318 tachyzoites.

319

320 Our analysis of the ER, nucleus, rhoptry and apicoplast in extracellular versus  
321 intracellular tachyzoites showed no consistent change in their cellular location or  
322 shape that coincided with the mitochondrial changes observed upon this  
323 transition (data not shown). This suggests that the interactions that exist between  
324 these organelles are not likely to contribute to the change of mitochondrial shape  
325 observed in our studies.

326 The predominant feature common to the three extracellular mitochondrial  
327 morphologies compared to intracellular mitochondria is a general retraction from

328 the periphery (Figure 5b), which correlates with a reduction in the number of  
329 patches where the mitochondrion is closely aligned to the IMC as observed by  
330 electron microscopy (Figure 6). In other eukaryotes, regions of mitochondrial  
331 juxtaposition to other organelles are often attributed to the function of tether  
332 complexes that enable direct transmission of signals and molecules between  
333 organelles. These regions are named membrane contact sites (MCS) and have  
334 been reported to be present between any two organelles that have been closely  
335 studied<sup>25,26</sup>. The areas of apposition observed in this study between the  
336 mitochondrion and the IMC have similar length, shape and distance to those  
337 described for MCS, and they persist for 10-30 minutes at least (Movie S7, Figure  
338 6d). We therefore hypothesize that mitochondrion-IMC MCS are one of the  
339 factors responsible for the peripheral positioning and shape of mitochondria in  
340 intracellular tachyzoites, and that they are reduced upon the transition to the  
341 extracellular matrix. This interaction may also explain the previous observation  
342 showing that upon tubulin disruption mitochondria associate with local  
343 concentrations of IMC<sup>9</sup>. This hypothesis is also supported by findings from the  
344 closely related parasite *Plasmodium falciparum*, where, in sporozoites, long  
345 linker molecules that are apparently derived from the subpellicular network  
346 underlying the IMC, link the IMC with mitochondria<sup>27</sup>.

347

348 Some of the well-studied MCS involve mitochondria and include the ER–  
349 Mitochondria Encounter Structure (ERMES)<sup>28</sup>, the ER Membrane protein  
350 Complex (EMC) that also functions in ER-mitochondria tethering<sup>29</sup>, and the

351 mitochondria and plasma-membrane tethering complex Num1p/Mdm36<sup>30</sup><sup>31</sup>.  
352 Mitochondrial contacts have also been observed with the yeast vacuole<sup>32</sup> and  
353 peroxisomes<sup>33</sup>.  
354 It is hypothesized that the IMC cisternae in Apicomplexa are of ER origin<sup>34</sup>  
355 raising the possibility that complexes that tether the ER and mitochondria in other  
356 organisms may also tether the IMC and mitochondria in *T. gondii*. While no  
357 homologs of the ERMES complex components are identifiable in *Toxoplasma*, a  
358 set of EMC proteins homologs is present<sup>35</sup>. It has been postulated that in  
359 evolutionary lineages lacking ERMES, the more evolutionarily conserved EMC  
360 mediates the ER–mitochondrion tether. In humans, four other complexes were  
361 proposed to mediate mitochondrial-ER tethering (reviewed in<sup>26</sup>). Components of  
362 those complexes include the dynamin-like protein Mfn2, the mitochondrial fission  
363 mediator Fis1 and the mitochondrial voltage dependent anion channel (VDAC),  
364 all of which have homologs in *T. gondii* (Table S1) and are candidates to mediate  
365 these potential contact sites. Alternatively, a novel complex that is specific to  
366 these parasites or to the group of organisms containing alveoli, may tether the  
367 IMC and mitochondrion. Identifying tethers and confirming the existence of  
368 mitochondrial MCS in *Toxoplasma* is now a major priority in the field of organelle  
369 contact sites, that otherwise focuses mainly on opisthokonts, as it would expand  
370 to understand their role in divergent eukaryotes.  
371  
372 The possibility of mitochondrial-IMC communication raises the question of what  
373 functions are supported via exchange between these two organelles. The most

374 commonly discussed functions of mitochondrial MCS are control of calcium  
375 homeostasis and trafficking of lipids. The lipid composition of the IMC and  
376 mitochondrion in *Toxoplasma* is not known. While lipid synthesis<sup>36 37</sup> and lipid-  
377 dependent signalling pathways<sup>38</sup> that are relevant to the function of both these  
378 organelles are being discovered, it is early to speculate on a potential role of  
379 mitochondrial-IMC contacts in lipid exchange.

380 Previous studies provide evidence both for and against a role for mitochondrion-  
381 IMC MCS in calcium homeostasis that may be similar to what is reported for  
382 mitochondrial-ER exchange in other systems. Regarding the mitochondria,  
383 *Toxoplasma* seems not to carry the gene encoding the mitochondrial calcium  
384 uniporter (MCU)<sup>38</sup> that is involved in Ca<sup>2+</sup> uptake in other systems. However, a  
385 mitochondrial antiporter which can mediate H<sup>+</sup>-coupled Ca<sup>2+</sup> exchange has a  
386 homolog in *Toxoplasma*<sup>39</sup>. As for the IMC, calcium storage in the *T. gondii*  
387 alveolar sacs has not been examined. However the alveoli of the related  
388 *Paramecium* spp act as calcium stores<sup>40</sup>, and this is also a suggested role of the  
389 IMC of the more closely related *Plasmodium* spp<sup>41</sup>.

390 MCS that mediate calcium homeostasis expand or reduce in respond to changes  
391 in calcium flux<sup>42</sup>. Treatments with ionomycin, which results in calcium flux in the  
392 parasite cytosol, induced a significant shift in the distribution of mitochondrial  
393 shapes (Figure 2c) that may be a result of change in contact site length or  
394 abundance. Importantly, the observed shift is moderate. Moreover, neither  
395 depletion of lipids nor a modification of the overall medium composition to mimic  
396 the intracellular ion environment resulted in alteration to the mitochondrial shapes

397 observed upon egress (Figure S5). We cannot therefore conclude that there is  
398 any specific strong correlation between any single condition that we have  
399 analyzed and mitochondrial morphology. In this context, it is important to note  
400 that as observed in other eukaryotes, the activity of multiple tethers, executing  
401 various functions, may well contribute to the overall interaction between the same  
402 two organelles. Our hypothesis is that the observed mitochondrial change upon  
403 egress is the result of multiple changes encountered in this transition.

404 In addition to ions and lipids, other known roles of MCS that may have an effect  
405 here include the control of mitochondrial inheritance after cell division, and the  
406 regulation of the function of enzymes that work in trans (e.g. enzymes present on  
407 one organelle but modify substrates found on the other).

408

409 Identification of the molecular machinery responsible for the establishment of the  
410 patches of mitochondrion-IMC proximity would enable tackling its functional  
411 significance and test the above hypotheses. Likewise, understanding whether the  
412 peripheral retraction observed in extracellular parasites serves a function for  
413 extracellular survival, and/or it is the result of an intracellular function that is  
414 reduced upon egress, is an important step in the way of elucidating its role.

415 This work identified specific morphological states that occur to the mitochondrion  
416 in extracellular parasites, which are distinct from other stress-induced  
417 mitochondrial changes that have been previously described. These measures  
418 can now be used to assess the outcome of genetic ablation of potential  
419 mitochondrial biogenesis control mechanisms to address future questions

420 designed to better understand why these remarkable changes in the  
421 mitochondrion take place.

422

423 **Methods**

424 **Parasite culture**

425 Parasites were grown in human foreskin fibroblasts (HFFs) in supplemented  
426 Dulbecco's modified Eagle's medium supplemented with 2mM L-Glutamine and  
427 10% Fetal Bovine Serum (we refer to this as "full medium"). To generate  
428 fluorescent stable lines IMC3-YFP and TGME49\_215430-tomato transgenes or  
429 an endogenous YFP tagging construct for TGME49\_215430 were introduced into  
430 the RH based F3-line<sup>43</sup>, following enrichment of the fluorescent population of  
431 parasites stably expressing these transgenes via cell sorting using the S3e cell-  
432 sorter (BioRad). Clones were isolated by limiting dilutions.

433

434 **Immunofluorescence assay**

435 All manipulations were carried out at room temperature. Intracellular parasites  
436 grown in HFFs seeded on glass coverslips were fixed with 4% paraformaldehyde  
437 for 20 minutes and washed in PBS. Extracellular parasites for  
438 immunofluorescence assay were placed onto poly-L-lysine coated coverslips and  
439 then fixed with 4% paraformaldehyde for 20 minutes and washed once with PBS.  
440 Cells were permeabilized and blocked in PBS/0.02% Triton-X-100/2% BSA  
441 (PBS/Triton/BSA) for 20 minutes. Slides were incubated for 60 minutes with  
442 primary antibodies: anti-TGME\_215430<sup>11</sup>; ISP1<sup>44</sup>; IMC1<sup>45</sup>; Tom40<sup>12</sup>; and tubulin  
443 (Sigma) in PBS/Triton/BSA, washed with 3xPBS/0.02% Triton-X-100 and  
444 incubated for 45 minutes with Alexa488- or Alexa594-conjugated goat anti-  
445 mouse or anti-rabbit IgGs in PBS/Triton/FBS. For Mitotracker® staining HFFs

446 with parasites on glass cover slips were incubated in 300nM Mitotracker® for  
447 30min at 37<sup>0</sup>c. For Oryzalin treatment intracellular parasites were cultured in  
448 presence of 2 uM Oryzalin for 18 hours after which the cells were fixed with 4%  
449 PFA for 20 minutes at RT and immunofluorescence assay was carried out as  
450 described above.

451

#### 452 **Fluorescent Microscopy**

453 Micrographs were obtained using DeltaVision Core microscope  
454 (AppliedPrecision) and processed using softWoRx and FIJI software. Parasites  
455 with heavily distorted cell shape and fragmented mitochondria were excluded  
456 from the analysis.

457 For super-resolution structural illumination microscopy (3D-SIM), stacks of 20-25  
458 images were taken with increments of 0.091 µm in a Zeiss Elyra PS.1 super-  
459 resolution microscope (Jena, Germany) with a 63x oil immersion objective using  
460 ZEN Black software (Zeiss, Germany). Three-phase SR-SIM images were  
461 reconstructed in the same software using Structural Illumination manual  
462 processing tool. Maximum projection SR-SIM images and 3D models were  
463 processed in Zen and FIJI softwares<sup>46</sup>.

464

#### 465 **Scoring Mitochondrial Morphology in Extracellular Parasites**

466 215430-YFP expressing parasites were released from HFFs by needle pass  
467 (23G, Henke Sass Wolf) and filtering through 3 µm filters (VWR, 515-2036).  
468 Parasites for immediate time point (Figure 2c, Figure S5) were centrifuged

469 (300RPM, 5 minutes) and fixed with 4% paraformaldehyde for 1 hour at room  
470 temperature. For egress in different medium compositions intracellular parasites  
471 are washed twice with the specific medium (12% full DMEM in Hanks-saline;  
472 FBS free medium; K<sup>+</sup> buffer), parasites are then mechanically released by needle  
473 pass, filter, centrifuge and fixed as above. For chemical egress (Figure 2c),  
474 intracellular parasites were incubated for 10 minutes in 2 µM ionomycin (Santa  
475 Cruz Biotechnology) in DMEM at 37° C prior to centrifugation and fixation. For the  
476 longer time points (Figure 4b) scraped, needle passed and filtered parasites were  
477 incubated in 37° C, 5% CO<sub>2</sub> in full medium for 6/12/24 hours before centrifugation  
478 and fixation. After fixation parasites were inoculated onto poly-L-lysine (Sigma)  
479 coated coverslips, allowed to adhere for 10 minutes at RT and washed once with  
480 PBS. Slides were mounted in DAPI Fluoromount-G® (Cambridge Bioscience)  
481 and stored at 4° C in the dark.

482 Morphologies were scored from micrographs obtained using DeltaVision Core  
483 microscope (Applied Precision) with x60 objective (example in Figure 2a).  
484 Parasites looking small and round and with swollen or fragmented mitochondria  
485 were excluded from the analysis also in the longer incubation where their  
486 numbers were high. All error bars are standard deviation (mean with SD). The  
487 data for each mitochondrial shape was compared to the same mitochondrial  
488 shape in the control population using paired (gliding and invasion) or unpaired  
489 (egress method and media requirements) t-test. For the ionomycin experiment  
490 the control is Full DMEM; for gliding and for invasion the control is the total

491 population counted from the same culture. For the 12% medium, FBS free  
492 medium and K<sup>+</sup> buffer the control is full DMEM.

493

494 **Invasion assay**

495 HFFs containing 215430-YFP expressing parasites were washed to remove  
496 extracellular parasites, and then scraped and needle pass (23G) to release  
497 parasites. Freshly release extracellular parasites were used to infect new HFFs  
498 on glass coverslips. Cells were fixed with 4% paraformaldehyde after 30 minutes  
499 of incubation at 37° C. Following wash in PBS, cells were incubated in 2% BSA in  
500 PBS for 20 minutes. Cells were then incubated with anti-SAG1 antibody (Abcam)  
501 in 2% BSA in PBS for 1 hour and then with Alexa594 antibodies in 2% BSA in  
502 PBS for 45 minutes. The slides were mounted in DAPI Fluoromount-G®  
503 (Cambridge Bioscience) and stored at 4° C in the dark. Micrographs were  
504 obtained using 3D-SIM as detailed above.

505

506 **Gliding assay**

507 HFFs containing 215430-YFP expressing parasites were washed to remove  
508 extracellular parasites, and then scraped and needle pass (23G) to release  
509 parasites. Freshly release extracellular parasites were inoculated on pre-coated  
510 poly-L-lysine (1:10 in PBS) glass bottom dish (Cellvis) at 4° C. The live dish was  
511 mounted on the imaging chamber of DeltaVision Core microscope  
512 (AppliedPrecision) preheated to 37° C. Images were taken every 7 seconds for a  
513 total of 10 minutes. Movie was compiled in FIJI software. For the movie used in

514 this manuscript the images were processed to account for cell drifting using the  
515 ImageJ plugin, StackReg, for recursive alignment  
516 (<http://bigwww.epfl.ch/thevenaz/stackreg/>).

517

518 **Egress assay**

519 HFFs containing 215430-YFP expressing parasites grown on glass bottom  
520 dishes (Cellvis) were washed to remove extracellular parasites. The dish was  
521 then mounted on the imaging chamber of DeltaVision Core microscope  
522 (AppliedPrecision) preheated to 37° C for live imaging. Images were taken every  
523 10 seconds for a total of 5 minutes and 2 µM ionomycin (Santa Cruz  
524 Biotechnology) was added after 2-4 time points were imaged. Movie was  
525 compiled in FIJI software.

526

527 **Electron microscopy**

528 RH strain *Toxoplasma* parasites expressing HA-tagged TgElp3 were prepared  
529 for immunoelectron microscopy (IEM) as previously described<sup>22</sup>. IEM processing  
530 and analysis was conducted by Wandy Beatty at Washington University, St.  
531 Louis. To immunolabel sections, a 1:25 dilution of rat anti-HA (Roche) was  
532 applied for 1 hour at room temperature. Samples were then incubated for another  
533 hour in a 1:30 dilution of goat anti-rat antibody conjugated to 18 nm colloidal gold  
534 (Jackson ImmunoResearch Laboratories) and stained with 5% uranyl acetate/2%  
535 methyl cellulose. Samples were analyzed on a JEOL 1200 EX transmission

536 electron microscope (JEOL USA Inc.) with an AMT 8 megapixel digital camera  
537 and AMT version 602 software (Advanced Microscopy Techniques).

538

539 **Transmission electron microscopy**

540 HFF infected cells and extracellular *T. gondii* tachyzoites were fixed with 2.5%  
541 glutaraldehyde and 4% paraformaldehyde in 0.1M phosphate buffer. Following  
542 serial washes in 0.1M phosphate buffer, the material was post-fixed in 1% OsO<sub>4</sub>  
543 (vol:vol) in the same buffer for 1 hour on ice in the dark, and contrasted en bloc  
544 with 0.5% aqueous uranyl acetate for 1 hour at room temperature in the dark.  
545 The samples were then dehydrated in acetone ascending series and embedded  
546 in epoxy resin. Ultra-thin sections (60nm) were observed in a Tecnai T20  
547 transmission electron microscope (FEI, Netherlands). Images were processed  
548 and analyzed in FIJI software<sup>46</sup>. For the mitochondrion-IMC proximity analysis,  
549 254 extracellular tachyzoites were imaged and 240 of infected HFFs. For the  
550 analysis, only distances less than 50 nm were considered as mitochondrion-IMC  
551 contact sites. The distances between IMC and mitochondrion profiles were  
552 measured in FIJI software, and data plotted in Microsoft Exel software.

553

554 **Electron tomography**

555 For 3D electron tomography, 200 nm-thick sections of infected HFFs were  
556 collected onto formvar-coated nickel grids. Images were recorded in tilt series  
557 covering +/- 60°, at 2° increment intervals in a Jeol 2200 transmission electron  
558 microscope (Jeol, Japan) operating at 200 kV equipped with a Gatan US4000

559 camera. Tilt series were aligned by cross correlation and tomogram  
560 reconstruction calculated by weighted back projection using Etomo from IMOD  
561 software package (Kremer et al., 1996). Segmentation and generation of the 3D  
562 model were performed using 3dmod program of the same software package  
563  
564

## 565      References

- 566
- 567      1      Collins, T. J. and Bootman, M. D., Mitochondria are morphologically  
568      heterogeneous within cells. *J Exp Biol* **206** (Pt 12), 1993 (2003).
- 569      2      Kasahara, A. et al., Mitochondrial fusion directs cardiomyocyte differentiation  
570      via calcineurin and Notch signaling. *Science* **342** (6159), 734 (2013).
- 571      3      Gorsich, S. W. and Shaw, J. M., Importance of mitochondrial dynamics during  
572      meiosis and sporulation. *Mol Biol Cell* **15** (10), 4369 (2004).
- 573      4      Priest, J. W. and Hajduk, S. L., Developmental regulation of mitochondrial  
574      biogenesis in *Trypanosoma brucei*. *J Bioenerg Biomembr* **26** (2), 179 (1994).
- 575      5      Schneider, A., Unique aspects of mitochondrial biogenesis in  
576      trypanosomatids. *Int J Parasitol* **31** (13), 1403 (2001).
- 577      6      Schnaufer, A., Clark-Walker, G. D., Steinberg, A. G., and Stuart, K., The F1-ATP  
578      synthase complex in bloodstream stage trypanosomes has an unusual and  
579      essential function. *EMBO J* **24** (23), 4029 (2005).
- 580      7      Melo, E. J., Attias, M., and De Souza, W., The single mitochondrion of  
581      tachyzoites of *Toxoplasma gondii*. *J Struct Biol* **130** (1), 27 (2000).
- 582      8      Seeber, F., Ferguson, D. J., and Gross, U., *Toxoplasma gondii*: a  
583      paraformaldehyde-insensitive diaphorase activity acts as a specific  
584      histochemical marker for the single mitochondrion. *Exp Parasitol* **89** (1), 137  
585      (1998).
- 586      9      Nishi, M., Hu, K., Murray, J. M., and Roos, D. S., Organellar dynamics during the  
587      cell cycle of *Toxoplasma gondii*. *J Cell Sci* **121** (Pt 9), 1559 (2008).
- 588      10     Konradt, C. et al., Endothelial cells are a replicative niche for entry of  
589      *Toxoplasma gondii* to the central nervous system. *Nat Microbiol* **1**, 16001  
590      (2016).
- 591      11     MacRae, J. I. et al., Mitochondrial metabolism of glucose and glutamine is  
592      required for intracellular growth of *Toxoplasma gondii*. *Cell Host Microbe* **12**  
593      (5), 682 (2012).
- 594      12     van Dooren, G. G., Yeoh, L. M., Striepen, B., and McFadden, G. I., The Import of  
595      Proteins into the Mitochondrion of *Toxoplasma gondii*. *J Biol Chem* **291** (37),  
596      19335 (2016).
- 597      13     Wang, Y., Weiss, L. M., and Orlofsky, A., Host cell autophagy is induced by  
598      *Toxoplasma gondii* and contributes to parasite growth. *J Biol Chem* **284** (3),  
599      1694 (2009).
- 600      14     Ghosh, D., Walton, J. L., Roepe, P. D., and Sinai, A. P., Autophagy is a cell death  
601      mechanism in *Toxoplasma gondii*. *Cell Microbiol* **14** (4), 589 (2012).
- 602      15     Lavine, M. D. and Arrizabalaga, G., Analysis of monensin sensitivity in  
603      *Toxoplasma gondii* reveals autophagy as a mechanism for drug induced  
604      death. *PLoS One* **7** (7), e42107 (2012).
- 605      16     Sheiner, L., Dowse, T. J., and Soldati-Favre, D., Identification of trafficking  
606      determinants for polytopic rhomboid proteases in *Toxoplasma gondii*. *Traffic*  
607      **9** (5), 665 (2008).
- 608      17     Labbe, K., Murley, A., and Nunnari, J., Determinants and functions of  
609      mitochondrial behavior. *Annu Rev Cell Dev Biol* **30**, 357 (2014).

- 610       <sup>18</sup> Sheiner, L., Vaidya, A. B., and McFadden, G. I., The metabolic roles of the  
611       endosymbiotic organelles of *Toxoplasma* and *Plasmodium* spp. *Curr Opin*  
612       *Microbiol* **16** (4), 452 (2013).
- 613       <sup>19</sup> Kobayashi, T. et al., Mitochondria and apicoplast of *Plasmodium falciparum*:  
614       behaviour on subcellular fractionation and the implication. *Mitochondrion* **7**  
615       (1-2), 125 (2007).
- 616       <sup>20</sup> Harding, C. R. and Meissner, M., The inner membrane complex through  
617       development of *Toxoplasma gondii* and *Plasmodium*. *Cell Microbiol* **16** (5),  
618       632 (2014).
- 619       <sup>21</sup> Mann, T. and Beckers, C., Characterization of the subpellicular network, a  
620       filamentous membrane skeletal component in the parasite *Toxoplasma*  
621       *gondii*. *Mol Biochem Parasitol* **115** (2), 257 (2001).
- 622       <sup>22</sup> Stilger, K. L. and Sullivan, W. J., Jr., Elongator protein 3 (Elp3) lysine  
623       acetyltransferase is a tail-anchored mitochondrial protein in *Toxoplasma*  
624       *gondii*. *J Biol Chem* **288** (35), 25318 (2013).
- 625       <sup>23</sup> Shaw, M. K., Compton, H. L., Roos, D. S., and Tilney, L. G., Microtubules, but not  
626       actin filaments, drive daughter cell budding and cell division in *Toxoplasma*  
627       *gondii*. *J Cell Sci* **113** ( Pt 7), 1241 (2000).
- 628       <sup>24</sup> Hliscs, M. et al., Organization and function of an actin cytoskeleton in  
629       *Plasmodium falciparum* gametocytes. *Cell Microbiol* **17** (2), 207 (2015).
- 630       <sup>25</sup> Elbaz, Y. and Schuldiner, M., Staying in touch: the molecular era of organelle  
631       contact sites. *Trends Biochem Sci* **36** (11), 616 (2011).
- 632       <sup>26</sup> Prinz, W. A., Bridging the gap: membrane contact sites in signaling,  
633       metabolism, and organelle dynamics. *J Cell Biol* **205** (6), 759 (2014).
- 634       <sup>27</sup> Kudryashev, M. et al., Positioning of large organelles by a membrane-  
635       associated cytoskeleton in *Plasmodium* sporozoites. *Cell Microbiol* **12** (3),  
636       362 (2010).
- 637       <sup>28</sup> Kornmann, B. et al., An ER-mitochondria tethering complex revealed by a  
638       synthetic biology screen. *Science* **325** (5939), 477 (2009).
- 639       <sup>29</sup> Lahiri, S. et al., A conserved endoplasmic reticulum membrane protein  
640       complex (EMC) facilitates phospholipid transfer from the ER to  
641       mitochondria. *PLoS Biol* **12** (10), e1001969 (2014).
- 642       <sup>30</sup> Klecker, T., Scholz, D., Fortsch, J., and Westermann, B., The yeast cell cortical  
643       protein Num1 integrates mitochondrial dynamics into cellular architecture. *J*  
644       *Cell Sci* **126** (Pt 13), 2924 (2013).
- 645       <sup>31</sup> Lackner, L. L. et al., Endoplasmic reticulum-associated mitochondria-cortex  
646       tether functions in the distribution and inheritance of mitochondria. *Proc*  
647       *Natl Acad Sci U S A* **110** (6), E458 (2013).
- 648       <sup>32</sup> Elbaz-Alon, Y. et al., A dynamic interface between vacuoles and mitochondria  
649       in yeast. *Dev Cell* **30** (1), 95 (2014).
- 650       <sup>33</sup> Cohen, Y. et al., Peroxisomes are juxtaposed to strategic sites on  
651       mitochondria. *Mol Biosyst* **10** (7), 1742 (2014).
- 652       <sup>34</sup> de Melo, E. J. and de Souza, W., A cytochemistry study of the inner membrane  
653       complex of the pellicle of tachyzoites of *Toxoplasma gondii*. *Parasitol Res* **83**  
654       (3), 252 (1997).

- 655      35 Wideman, J. G. and Munoz-Gomez, S. A., The evolution of ERMIONE in  
656      mitochondrial biogenesis and lipid homeostasis: An evolutionary view from  
657      comparative cell biology. *Biochim Biophys Acta* (2016).
- 658      36 Bisanz, C. et al., *Toxoplasma gondii* acyl-lipid metabolism: de novo synthesis  
659      from apicoplast-generated fatty acids versus scavenging of host cell  
660      precursors. *Biochem J* **394** (Pt 1), 197 (2006).
- 661      37 Hartmann, A. et al., Phosphatidylethanolamine synthesis in the parasite  
662      mitochondrion is required for efficient growth but dispensable for survival of  
663      *Toxoplasma gondii*. *J Biol Chem* **289** (10), 6809 (2014).
- 664      38 Bullen, H. E. et al., Phosphatidic Acid-Mediated Signaling Regulates  
665      Microneme Secretion in Toxoplasma. *Cell Host Microbe* **19** (3), 349 (2016).
- 666      39 Rotmann, A. et al., PfCHA is a mitochondrial divalent cation/H<sup>+</sup> antiporter in  
667      *Plasmodium falciparum*. *Mol Microbiol* **76** (6), 1591 (2010).
- 668      40 Ladenburger, E. M., Sehring, I. M., Korn, I., and Plattner, H., Novel types of  
669      Ca<sup>2+</sup> release channels participate in the secretory cycle of Paramecium cells.  
670      *Mol Cell Biol* **29** (13), 3605 (2009).
- 671      41 Holder, A. A., Mohd Ridzuan, M. A., and Green, J. L., Calcium dependent  
672      protein kinase 1 and calcium fluxes in the malaria parasite. *Microbes Infect*  
673      **14** (10), 825 (2012).
- 674      42 Idevall-Hagren, O., Lu, A., Xie, B., and De Camilli, P., Triggered Ca<sup>2+</sup> influx is  
675      required for extended synaptotagmin 1-induced ER-plasma membrane  
676      tethering. *EMBO J* **34** (17), 2291 (2010).
- 677      43 Sheiner, L. et al., A systematic screen to discover and analyze apicoplast  
678      proteins identifies a conserved and essential protein import factor. *PLoS*  
679      *Pathog* **7** (12), e1002392 (2011).
- 680      44 Beck, J. R. et al., A novel family of Toxoplasma IMC proteins displays a  
681      hierarchical organization and functions in coordinating parasite division.  
682      *PLoS Pathog* **6** (9), e1001094 (2010).
- 683      45 Wighroski, M. J. et al., Clostridium septicum alpha-toxin is active against the  
684      parasitic protozoan *Toxoplasma gondii* and targets members of the SAG  
685      family of glycosylphosphatidylinositol-anchored surface proteins. *Infect*  
686      *Immun* **70** (8), 4353 (2002).
- 687      46 Schindelin, J. et al., Fiji: an open-source platform for biological-image  
688      analysis. *Nat Methods* **9** (7), 676 (2012).
- 689      47 Sadak, A., Taghy, Z., Fortier, B., and Dubremetz, J. F., Characterization of a  
690      family of rhoptry proteins of *Toxoplasma gondii*. *Mol Biochem Parasitol* **29** (2-  
691      3), 203 (1988).
- 692      48 Agrawal, S., van Dooren, G. G., Beatty, W. L., and Striepen, B., Genetic evidence  
693      that an endosymbiont-derived endoplasmic reticulum-associated protein  
694      degradation (ERAD) system functions in import of apicoplast proteins. *J Biol*  
695      *Chem* **284** (48), 33683 (2009).
- 696  
697  
698  
699  
700

701   **Acknowledgment**

702  
703   We thank Ross Waller and Silvia Moreno for critical review of the manuscript. LS  
704   is a Royal Society of Edinburgh personal research fellow. The work is funded by  
705   BBSRC BB/N003675/1 and by the Wellcome Trust grant 097821/Z/11/Z (To L.S),  
706   by National Institutes of Health Grant AI116496 (to W. J. S.), American Heart  
707   Association Predoctoral Fellowship Grant 12PRE11940015 (to K. L. S.), and  
708   Indiana Clinical and Translational Sciences Institute (CTSI) Career Development  
709   Award PHS (NCCR) 5TL1RR025759-03 (to K. L. S.). The Wellcome Centre for  
710   Molecular Parasitology is supported by core funding from the Wellcome Trust  
711   [ref: 104111]. Finally, we also thank Wandy Beatty (Washington University) for  
712   assistance with IEM and David Bhella (University of Glasgow) for assistance with  
713   tomogram acquisition.

714

715

716

717   **Author Contributions**

718

719   L.S. conceived and designed the study, interpreted the data and wrote the paper.  
720   L.L. performed and analyzed the transmission electron microscopy and  
721   contributed to writing the manuscript. J.O. optimized live microscopy conditions,  
722   developed morphology scoring system, designed and implemented all other  
723   experimental details and contributed to writing the manuscript. KLS generated  
724   TgElp3 expressing parasites and provided immune-EM data. WJS designed  
725   TgElp3 studies and contributed to writing the manuscript.

726

727   **Competing Financial Interest Declaration**

728

729   The authors read and understood NPG policy on competing financial interest  
730   (<http://www.nature.com/authors/policies/competing.html>) and we declare no  
731   competing financial interests.

732

733 **Figure 1 A new peripheral marker defines additional mitochondrial**  
734 **structures to a matrix marker.** Immunofluorescence micrograph of the  
735 mitochondria of two intracellular *T. gondii* tachyzoite expressing 215430-YFP  
736 (green) and stained with anti-Tom40 antibody (**a**) or Mitotracker® (**b**). All panels  
737 show Z projection. (**c,d**) Immunofluorescence micrograph of the mitochondria of  
738 two intracellular *T. gondii* tachyzoite expressing HSP60-RFP (magenta) and  
739 215430-YFP (green). All panels show Z projection. Arrowhead in (**c**) highlight an  
740 example of 215430 marking additional structures to the matrix marker.  
741 Arrowheads in (**d**) point to places where the matrix signal break and the 215430  
742 signal is continues. Bars 2μm.  
743

744 **Figure 2 Mitochondrial morphology of *T. gondii* tachyzoites changes upon**  
745 **host cell egress.** (**a**) Fluorescence micrograph of intracellular (In) and  
746 extracellular (out) populations of *T. gondii* tachyzoites taken utilizing the signal  
747 from 215430-YFP (green in the merge with the brightfield, top panels, and in the  
748 bottom panels). Bars 5μm. (**b**) Three representative images of each of the  
749 observed shapes of mitochondria in extracellular parasites and their  
750 classification. Each example shows the fluorescent signal image on the left and  
751 the merge of fluorescence and brightfield on the right. The color-coding of the  
752 frame (lasso – green; sperm-like – orange; collapsed – red) is maintained  
753 throughout all the figures. (**c**) Proportions of the morphologies scored in  
754 intracellular parasites (Intracellular, 776 parasites, over 6 independent  
755 experiments); in parasites mechanically released from host cell into full growth  
756 medium (Full, 864 parasites, over 9 independent experiments) or into diluted  
757 growth medium (12%, 653 parasites, over 2 independent experiments)  
758 immediately after release; and in parasites induced to egress by 2μM ionomycin  
759 (Ionomycin, 1177 parasites, over 6 independent experiments) immediately after  
760 release. Error bars are standard deviation. (**d**) Super-resolution microscopy  
761 images of the mitochondrial lasso morphology in intracellular (left) and the three  
762 main mitochondrial morphologies observed in extracellular: lasso, sperm-like and  
763 collapsed (right) shown as projection of all Z stacks (top) and as 3D  
764 reconstruction (bottom). 215430 - green. DAPI - blue. Bar 2μm.  
765

766 **Figure 3. The change in the mitochondrial morphology of extracellular**  
767 **tachyzoites is seen in motile and in actively invading parasites.** (**a**) A  
768 scheme depicting the main stages of the tachyzoite lytic cycle. (**b**) Snapshots  
769 from time-lapse microscopy of gliding parasites with different mitochondrial  
770 morphologies (Movie S3). Each parasite is numbered to enable following its  
771 trajectory. Time points (min:sec) are shown in each of the images. Bar - 10μm.  
772 (**c**) Distribution of lasso, sperm-like and collapsed morphologies in motile  
773 parasites (148 over 4 independent experiments), compared to the distribution in  
774 the total extracellular population (e.g. motile + non-motile, 171 parasites over the  
775 same 4 experiments), and to the distribution scored in intracellular parasites in  
776 the experiment presented in Figure 2c. (**d**) Fluorescence images of invading  
777 parasites with lasso (left), sperm-like (middle) and collapsed (right) mitochondria.  
778 Snapshots from movies S4.1/2/3. TGME49\_ 215430 (green). SAG1 (magenta)

779 staining was obtained without permeabilisation to visualize parasite that are half  
780 way into the host (i.e. only the extracellular part of the parasites is accessible to  
781 SAG1 antibody) as depicted in the scheme on the left. Bars - 1 $\mu$ m. (e)  
782 Distribution of mitochondrial morphologies in invading parasites (223 over 3  
783 independent experiments) that were allowed to invade immediately after  
784 mechanical release from host cells, compared to the population of extracellular  
785 parasites (621 over 3 independent experiments) obtained from the same  
786 preparation of egressed parasites, and to the distribution scored in intracellular  
787 parasites in the experiment presented in Figure 2c. Error bars in (c) and (e) are  
788 standard deviation.

789  
**Figure 4. The observed morphological change is reversible upon host cell**  
790 **invasion and directional.** (a) Snapshots from time-lapse microscopy of a  
791 parasite with collapsed mitochondrion after invasion and until completion of the  
792 first round of division (from Movie S5). 215430-YFP – green. IMC3 – magenta.  
793 Bar - 2 $\mu$ m. (b) Proportions of morphologies scored in parasites mechanically  
794 released from host cell after 6/12/24 hours of extracellular incubation (404, 930,  
795 419 parasites were scored over 3,9,3 independent experiments respectively).  
796 These are compared to scores obtained immediately after release or in  
797 intracellular parasites from the experiment shown in Figure 2c. Error bars are  
798 standard deviation. (c) Proportion of basal facing and apical facing “tail” in  
799 sperm-like mitochondria (190 parasites over 3 independent experiments, all  
800 counted after 6 hours of extracellular incubation, the time point with most sperm-  
801 like morphologies). The immunofluorescence on the right demonstrates  
802 examples of basal and apical facing tails. TGME49\_ 215430 – green. ISP1 –  
803 magenta. DAPI - blue. Bar - 1 $\mu$ m.

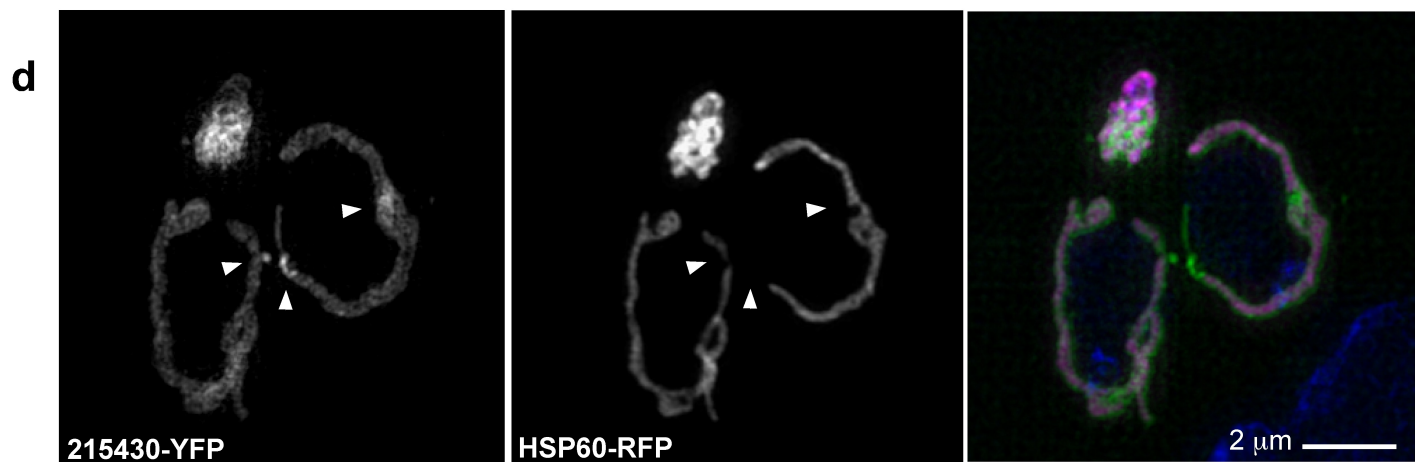
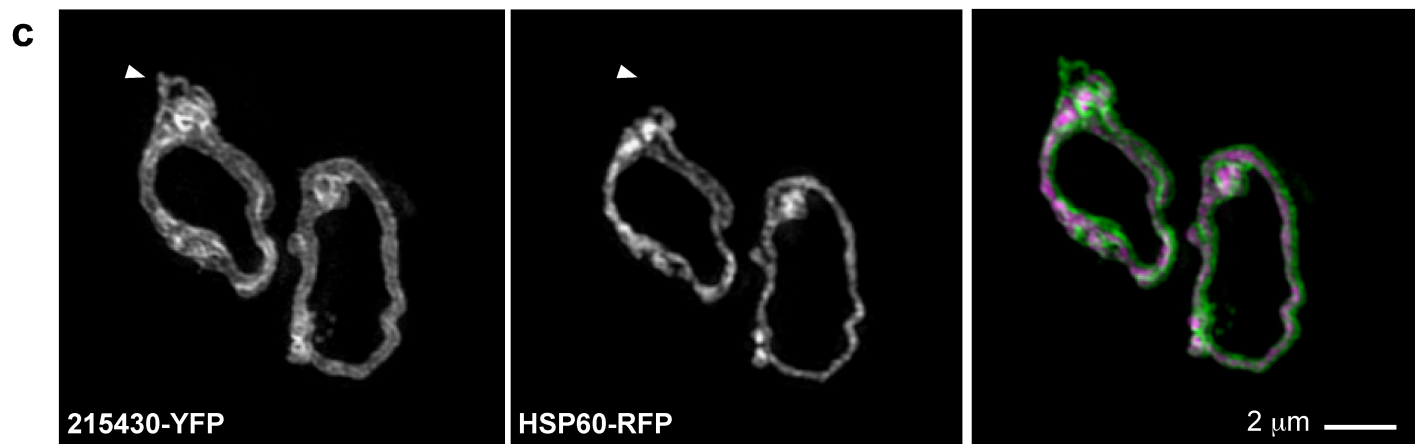
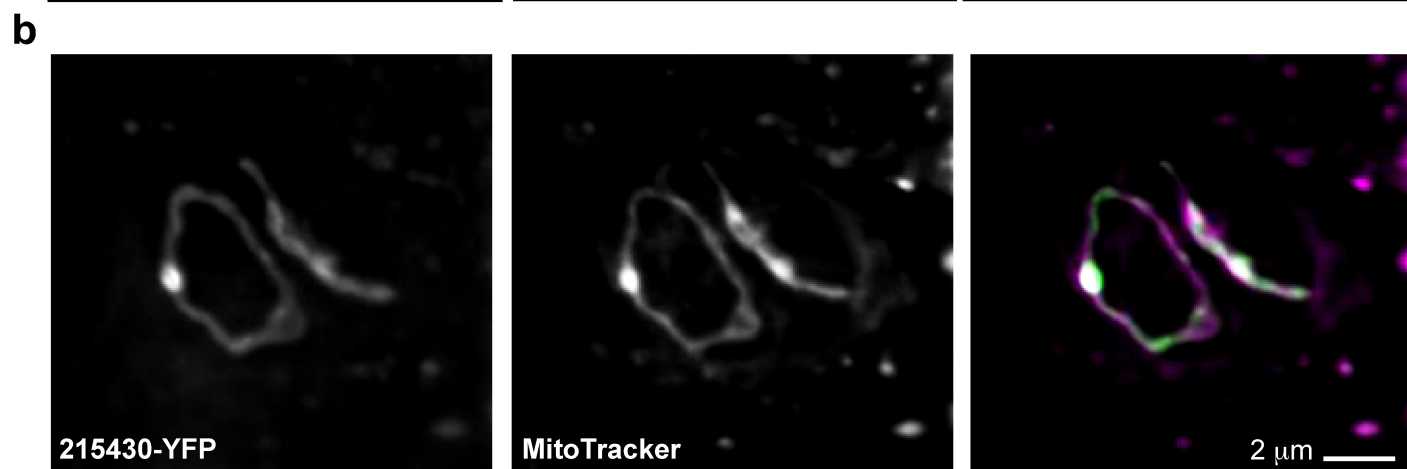
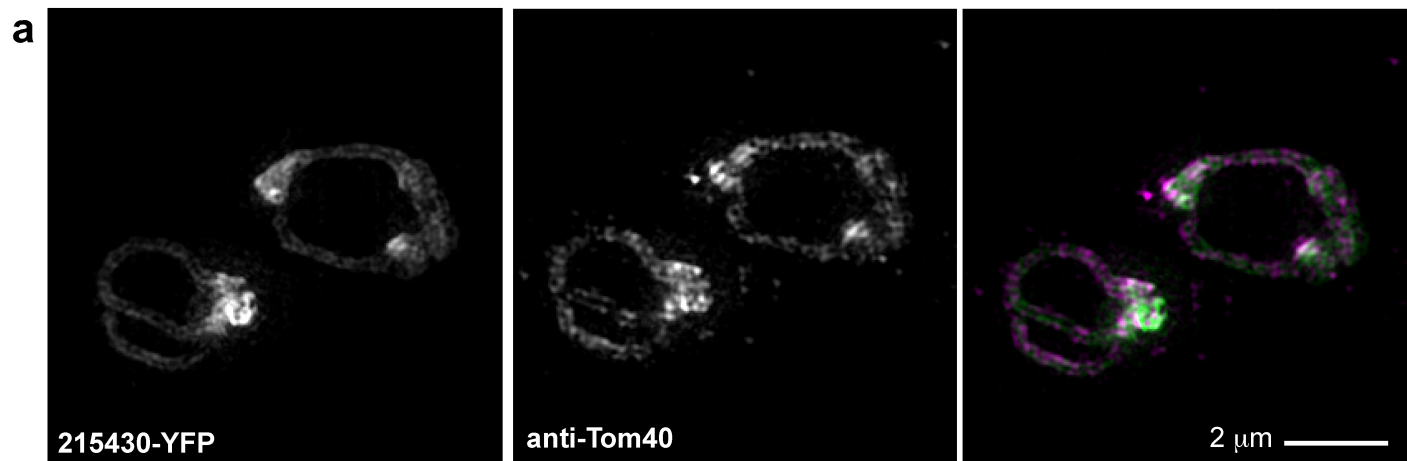
804  
805  
806  
**Figure 5. Analysis of morphology and positioning of other organelles in**  
807 **relation to the observed mitochondrial change reveals retraction from the**  
808 **parasite periphery as the main consistent feature of this change.** (a)

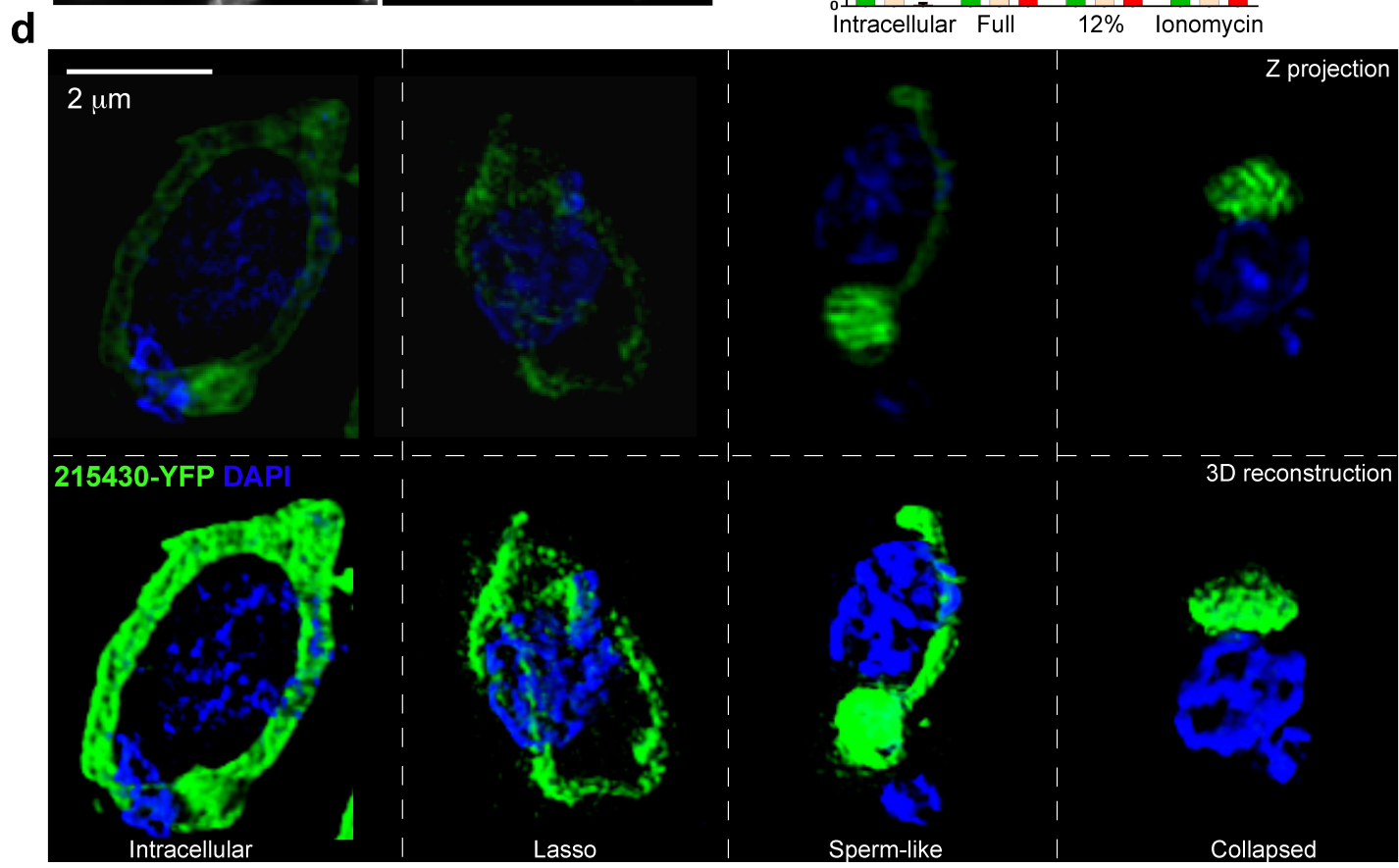
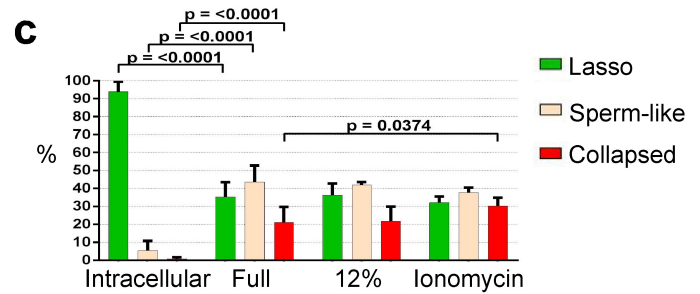
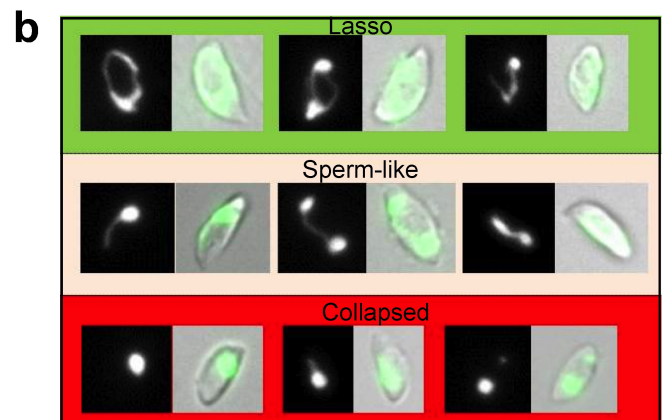
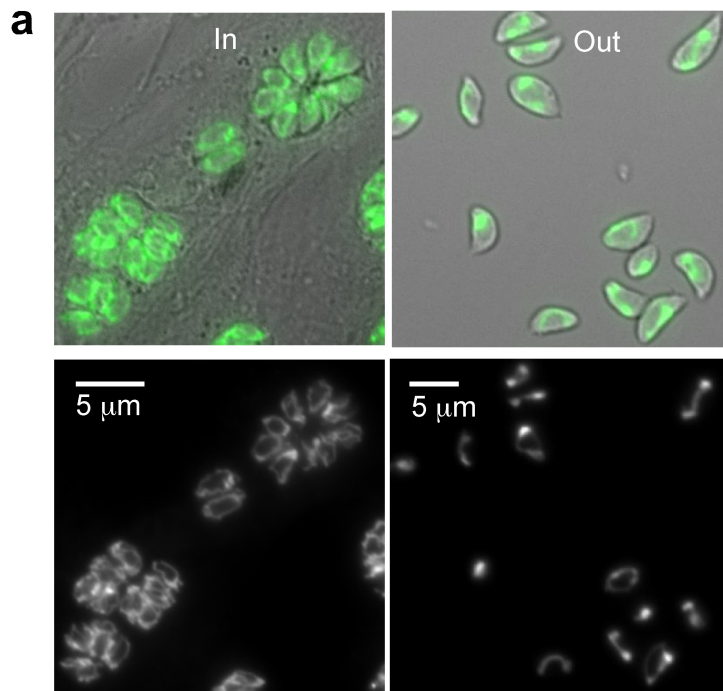
809 Randomly selected micrographs of the co-staining of mitochondrion and (i)  
810 nucleus (ii) apicoplast (iii) rhoptries (vi) ER in intracellular (in) and extracellular  
811 (out) parasites. (b) Representative micrographs of the co-staining of  
812 mitochondrion and IMC in intracellular (in) and extracellular (out) parasites. Bars  
813 - 2 $\mu$ m. TGME49\_ 215430 - green. Anti-Rop4 antibody (Rop2,4 - T34A7<sup>47</sup>),/Der-  
814 GFP<sup>48</sup>/DAPI/anti-CPN60 – magenta.

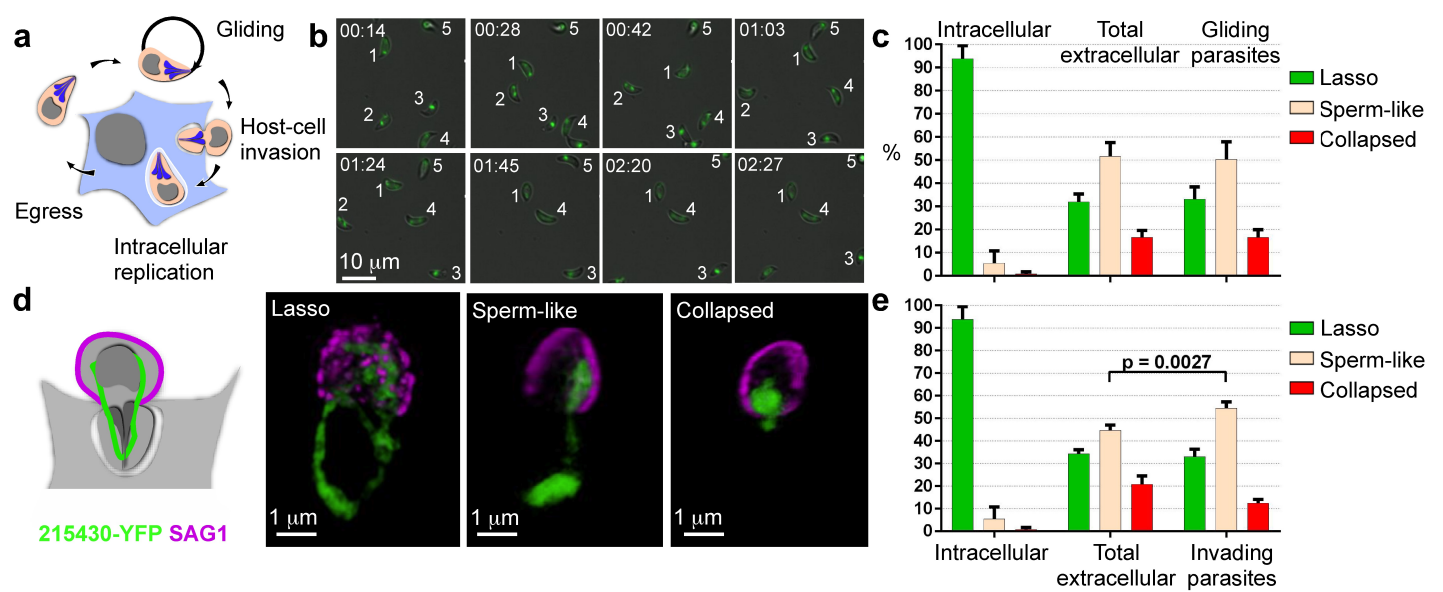
815  
816  
817  
**Figure 6. Mitochondrial peripheral retraction is linked to reduction in IMC**  
818 **tight-proximity zones.** (a) Schematic depiction of two tachyzoites showing their  
819 mitochondria (green), plasma membrane (grey), microtubules (dark purple), inner  
820 membrane complex (magenta) and sub pellicular microtubules (fuzzy grey). (b)

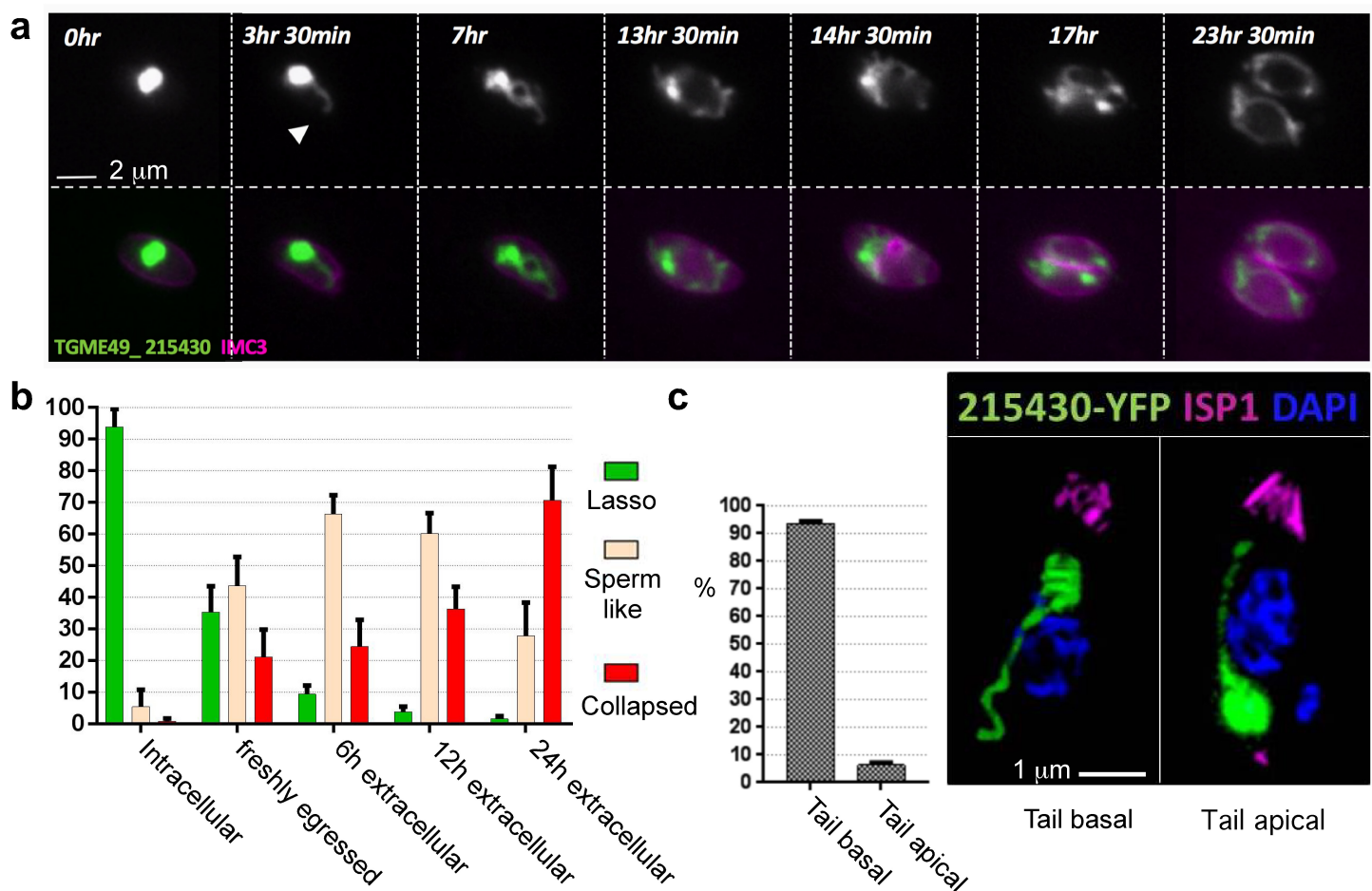
821 Cryo-immuno-EM using parasites expressing the mitochondrial associated  
822 TgElp3-HA<sup>22</sup>(labeled with gold beads). White arrows show IMC. Black arrows  
823 show the plasma membrane. (c) Frequency of sections showing patches of

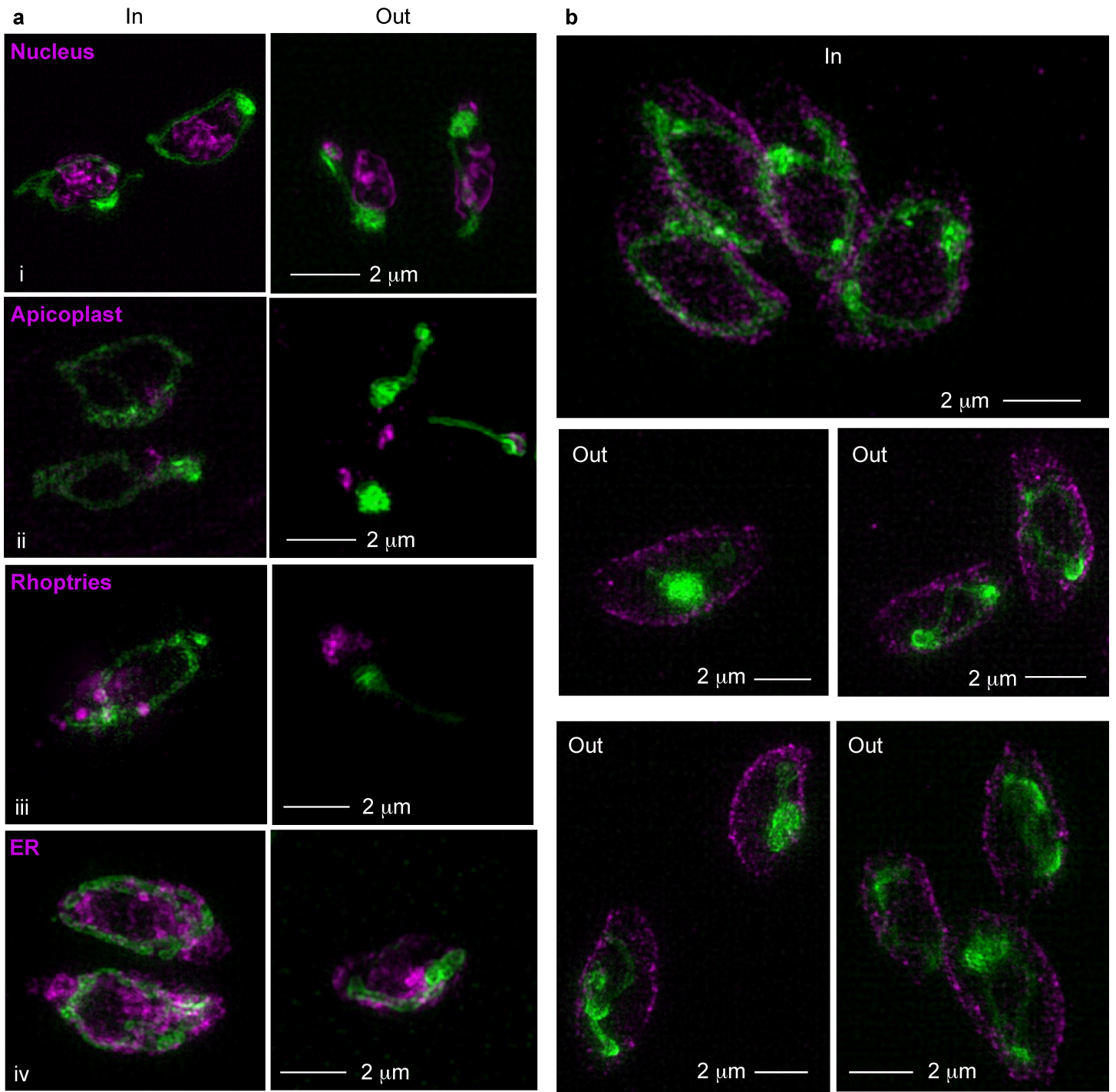
825 mitochondrial–IMC proximity of <50nm or >50nm distance and of section not  
826 showing mitochondrial profile, among EM sections of intracellular and  
827 extracellular parasites. **(d)** Snapshots from the time-lapse microscopy shown in  
828 Movie S7. Merge panel shows TGME49\_215430 in green and IMC3 in magenta,  
829 and each channel is also shown separately (IMC in the middle and TGME49\_  
830 215430 at the bottom). Square parentheses highlight regions of close IMC-  
831 mitochondrion contact that are stable over the period of live imaging. Arrowheads  
832 mark region of transient extensions from the mitochondrial tubule.  
833

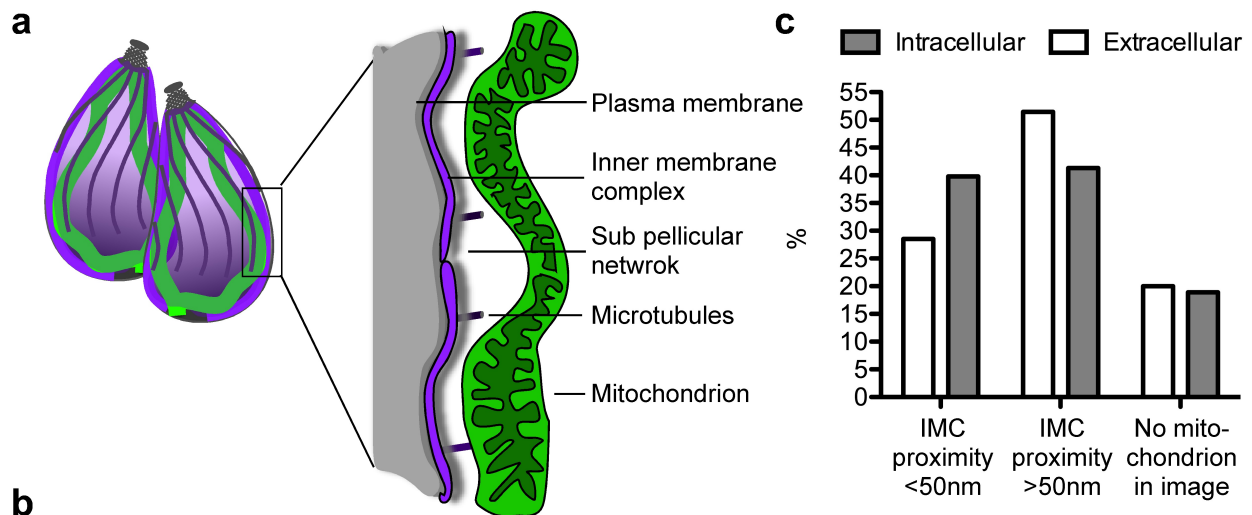




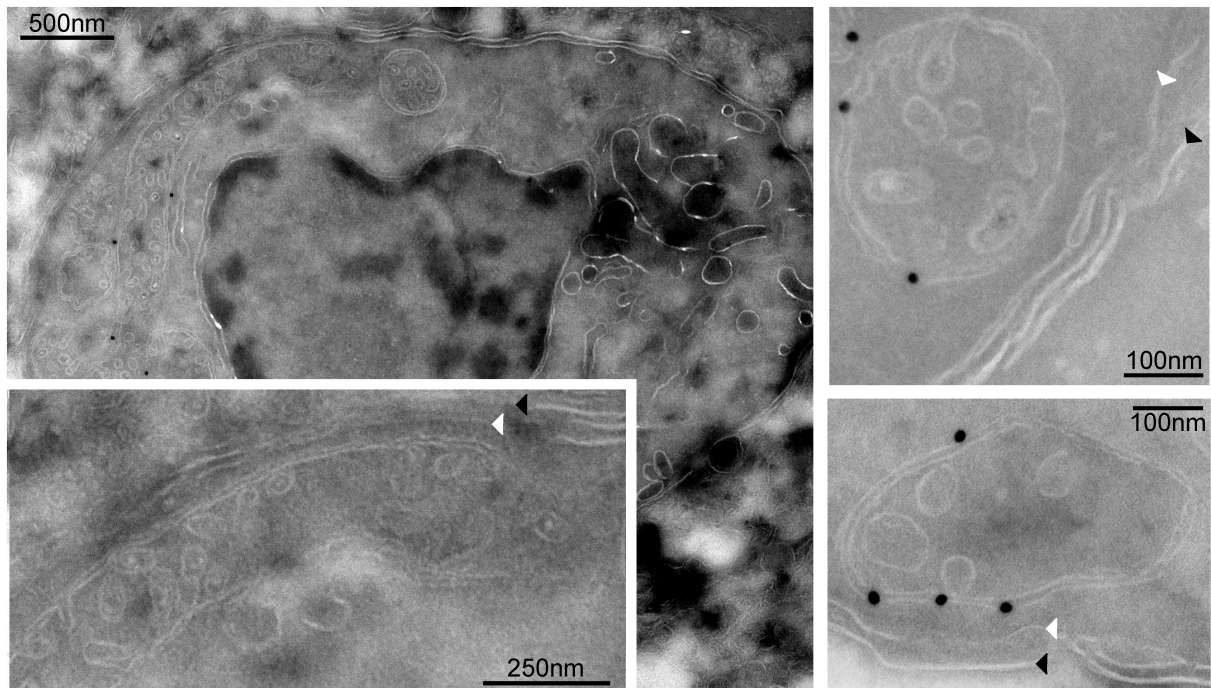








**b**



**d**

